Journal of Sustainable Metallurgy (2022) 8:1358–1369
https://doi.org/10.1007/s40831-022-00570-4

RESEARCH ARTICLE

Study on the High-Temperature Sintering Characteristics and Sintering Mechanism of Sea Sand Vanadium Titanomagnetite Based on Micro-sintering

Zhenxing Xing[1,2] · Jie Ma[1,2] · Gongjin Cheng[1,2] · He Yang[1,2] · Xiangxin Xue[1,2,3,4]

Received: 28 April 2022 / Accepted: 15 July 2022 / Published online: 15 August 2022

Abstract

The sea sand vanadium titanomagnetite has the problems of coarse particles, difficult agglomeration, and poor sintering performance. It is difficult for iron and steel enterprises to use it as an ironmaking raw material in large quantities. In this work, different methods were adopted to optimize the high-temperature sintering characteristics of sea sand vanadium titanomagnetite to increase the usage of sea sand ore. Based on the characterization and analysis of the basic physical and chemical properties of sea sand ore, the effects of adding limestone, ludwigite, and fine powder on the high-temperature sintering characteristics of sea sand ore were discussed. The proportion of sea sand ore was varied and its effect on the high-temperature sintering characteristics was studied. The phase composition and microstructure of sintered blocks with sea sand ore were analyzed by XRD and SEM–EDS, and the high-temperature sintering mechanism was studied. The results show that the high-temperature sintering characteristics of sea sand ore can be optimized to a certain extent by adding limestone, ludwigite, and fine powder. It is suggested that 15–35 wt% of sea sand ore was appropriate. The experimental results provided some reference methods for iron and steel enterprises to improve the utilization rate of sea sand ore in the actual sintering process.

Graphical Abstract

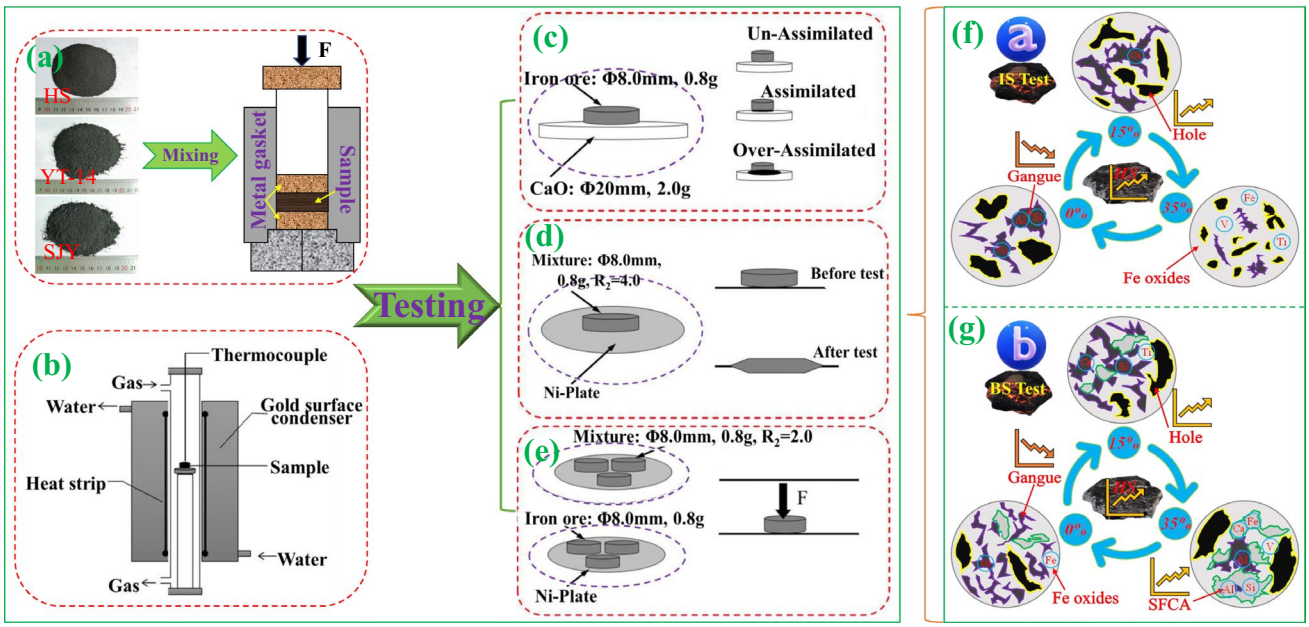

The contributing editor for this article was Il Sohn.

Extended author information available on the last page of the article

Keywords High-temperature sintering characteristics · Sea sand vanadium titanomagnetite · Sinter · Micro-sintering · Sintering mechanism

Abbreviations

AT	Assimilation temperature (°C)
LF	Liquid fluidity
BS	Binder strength (N)
IS	Intergranular strength (N)
TTM	Titanomagnetite
SFCA	Silico-ferrite of calcium and aluminum

Introduction

Vanadium titanomagnetite is a kind of multi-symbiotic iron ore mainly composed of iron, accompanied by vanadia–titania and various valuable elements (such as chromium, cobalt, nickel, and scandium), and it is also a kind of mineral resources with large reserves and wide distribution [1]. Different types of vanadium titanomagnetite resources have been found all over the world. China is the first country in the world to realize blast furnace smelting of vanadium titanomagnetite [2]. In recent years, the high-quality iron ore resources are gradually decreasing, and the prices of raw materials such as iron ore are rising, which forces iron and steel enterprises to try to use the sea sand vanadium titanomagnetite resources with low price and high comprehensive utilization value, to reduce the production cost [3].

Sea sand vanadium titanomagnetite is a complex iron ore resource with titanomagnetite (TTM) as the main ore phase formed by erosion. There are low-priced, easy-to-mine, and rich reserves, distributed in Japan, the Philippines, Indonesia, Australia, New Zealand, and the coastal areas of Hainan Island in China. At present, it is the second largest marine mineral mining industry, second to seabed oil [4–6]. Sea sand vanadium titanomagnetite is a kind of iron ore resource with a dense structure and complex distribution of valuable metal minerals. It is also recognized as a hard-to-beneficiate and hard-to-smelt mineral in the world [7]. Sea sand vanadium titanomagnetite has regular-shaped particles with a smooth and dense surface. Its particles have high hardness and melting point. It is difficult to granulate these particles during the process of pelletizing [8–10]. Compared with other iron ores, it has a smaller specific surface area, lower wettability, poorer hydrophilicity, poorer ball milling, and pelletizing performance. Therefore, it is not a preferred raw material in the large-scale iron and steel industry. Most of the related studies focused on the pre-oxidation treatment and reduction of sea sand raw ore [11–13].

The traditional sintering research of iron ore powder mainly focuses on normal temperature indexes such as chemical composition and physical properties. This evaluation method lacks comprehensive research on the characteristics of iron ore powder, especially the high-temperature physical and chemical characteristics reflected by iron ore powder in the sintering process. Therefore, it is difficult to reasonably select and utilize various iron ore powders [14, 15]. Some scholars have found that the sintering effect is related to the characteristics of various iron ore powders at high temperatures [16–18]. Wu et al. proposed the basic characteristics of iron ore powder sintering and systematically studied the high-temperature physical and chemical characteristics of iron ore powder at high temperature, providing a new idea for further optimization of the sintering process [19–21]. Zhang et al. studied the basic characteristics of Australian iron ore concentrate and its effects on sintering properties in the high-limonite sintering process. The effects of iron sand ratios on the basic characteristics of vanadium titanium mixed ores were investigated using micro-sinter and grey relational analysis methods. Their results indicated that the iron–sand ratio in vanadium–titanium mixed ores should be controlled within 9–12 wt% [22–24]. The above research mainly focused on the high-temperature sintering characteristics of single ore powder or mixed ore powder. There are very few researches on optimizing the high-temperature sintering characteristics of iron ore powder with additives, especially on optimizing the high-temperature sintering characteristics and sintering mechanism of sea sand vanadium titanomagnetite.

Based on the particularity of sea sand, this study attempts to investigate the high-temperature sintering characteristics and sintering behavior of sea sand ore under different conditions, to improve the proportion of sea sand ore in the preparation of sinter. The effects of adding a certain amount of limestone, ludwigite, and fine powder on the high-temperature sintering characteristics of sea sand ore were studied by a micro-sintering experiment. Sinter blocks were prepared with the help of the micro- sintering experiment, and the micro-morphology was analyzed. The study is aimed to investigate the optimum content of the sea sand ore and the additives.

Materials and Methods

Experimental Materials

The raw materials used in this experiment mainly include New Zealand Sea sand (HS), Sijiaying (SJY), and Yuantong-14 (YT-14). The experimental raw materials were quantitatively analyzed by an X-ray fluorescence

spectrometer (ZSXPrimus-II, Rigaku, Japan). The results are shown in Table 1. It can be observed from Table 1 that the total iron content of sea sand ore is 58.36 wt%, the contents of TiO_2 and V_2O_5 are 6.95 wt% and 0.47 wt%, respectively, which belongs to a typical vanadium titanomagnetite. The total iron content of Sijiaying (SJY) is 65.29 wt%, containing less TiO_2 and V_2O_5, which can be regarded as ordinary iron ore powder. Yuantong-14 (YT-14) has the highest total iron content of 66.27 wt%, and the contents of TiO_2 and V_2O_5 are 2.48 wt% and 0.29 wt%, respectively, which belongs to a kind of vanadia–titania iron ore powder.

Characteristic Analysis of Raw Materials

The XRD (X'Pert Pro; PANalytical, Almelo, The Netherlands) was used to analyze the phase composition of the experimental raw materials, and the results are shown in Fig. 1a. Sea sand ore is mainly composed of hematite (Fe_2O_3), magnetite (Fe_3O_4), and titanomagnetite (Fe_2TiO_4). Titanium is mainly present in sea sand ore in the form of titanomagnetite. Titanomagnetite (TTM) refers to a class of spinel oxides with the stoichiometry $Fe_{3-x}Ti_xO_4$, where $0 \le x \le 1$ [25, 26]. This describes a continuous solid solution series between the endpoints of magnetite ($x = 0$) and ulvöspinel ($x = 1$) [27, 28]. The Fe:Ti ratio obtained from Table 1 is consistent with a TTM ($Fe_{3-x}Ti_xO_4$), with a value of $x = 0.12$. The main phases of SJY are hematite (Fe_2O_3), magnetite (Fe_3O_4), and silica (SiO_2), while Yuantong-14 (YT-14) is mainly composed of hematite (Fe_2O_3), magnetite (Fe_3O_4), and titanomagnetite ($Fe_{2.5}Ti_{0.5}O_4$).

The particle size distribution of the three raw materials was used to analyze a laser particle size analyzer (Mastersizer 3000; Malvern, UK), and the results are shown in Fig. 1b. It can be observed from the particle size distribution diagram that the particle size of the sea sand ore is coarsest, followed by YT-14 ore, and SJY ore is the finest. Among them, the particle size distribution of the large part of sea sand ore is about 144 μm, and the particle size of YT-14 and SJY is relatively fine, most of which were distributed around 67 μm and 52 μm, respectively.

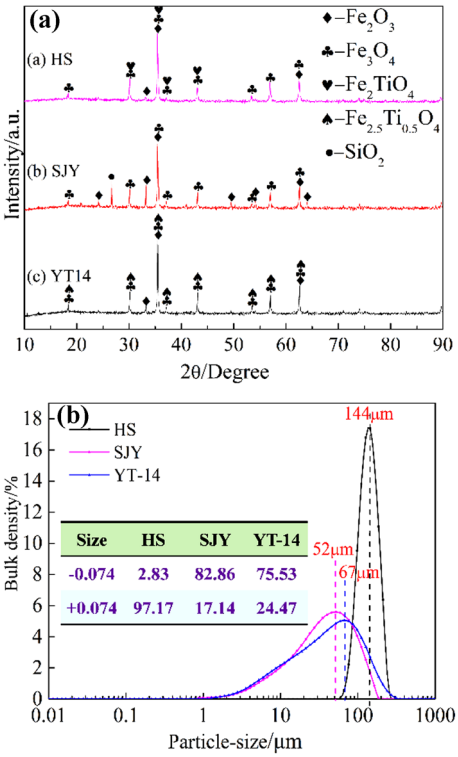

Fig. 1 The X-ray diffraction analysis diagram and particle size distribution diagram of experimental raw materials: **a** X-ray diffraction analysis of sea sand ore; **b** Particle size distribution diagram

Experimental Methods

The micro-sintering method qualitatively simulates the physical and chemical changes of minerals and the formation of sintering liquid phase in the high-temperature sintering process of iron ore powder. Infrared heating is adopted in the process, eliminating the need of fuel. Figure 2 shows the flowchart of the high-temperature sintering experiment, which mainly includes sample preparation (Fig. 2a), high-temperature sintering (Fig. 2b), and performance testing (Fig. 2d–f). The high-temperature physical and chemical characteristics measuring system (RHL-45) of iron ore powder used in this experiment is shown in Fig. 2b, and Fig. 2c shows the temperature heating curve in the high-temperature sintering process.

Table 1 Chemical composition of experimental raw materials (wt%)

Compositions	TFe	FeO	SiO_2	CaO	MgO	Al_2O_3	TiO_2	V_2O_5
Sea sand ore	58.36	28.23	3.27	1.15	2.88	3.33	6.95	0.47
SJY	65.29	17.99	6.72	0.22	0.42	0.42	0.12	0.03
YT-14	66.27	24.77	1.83	0.69	0.88	1.41	2.48	0.29
PB powder	61.76	21.45	3.66	0.32	0.32	1.96	0.43	0.02
Limestone	–	–	3.42	60.80	2.87	1.11	–	–
Ludwigite	51.47	6.34 (B_2O_3)	5.33	0.32	12.65	0.36	–	–

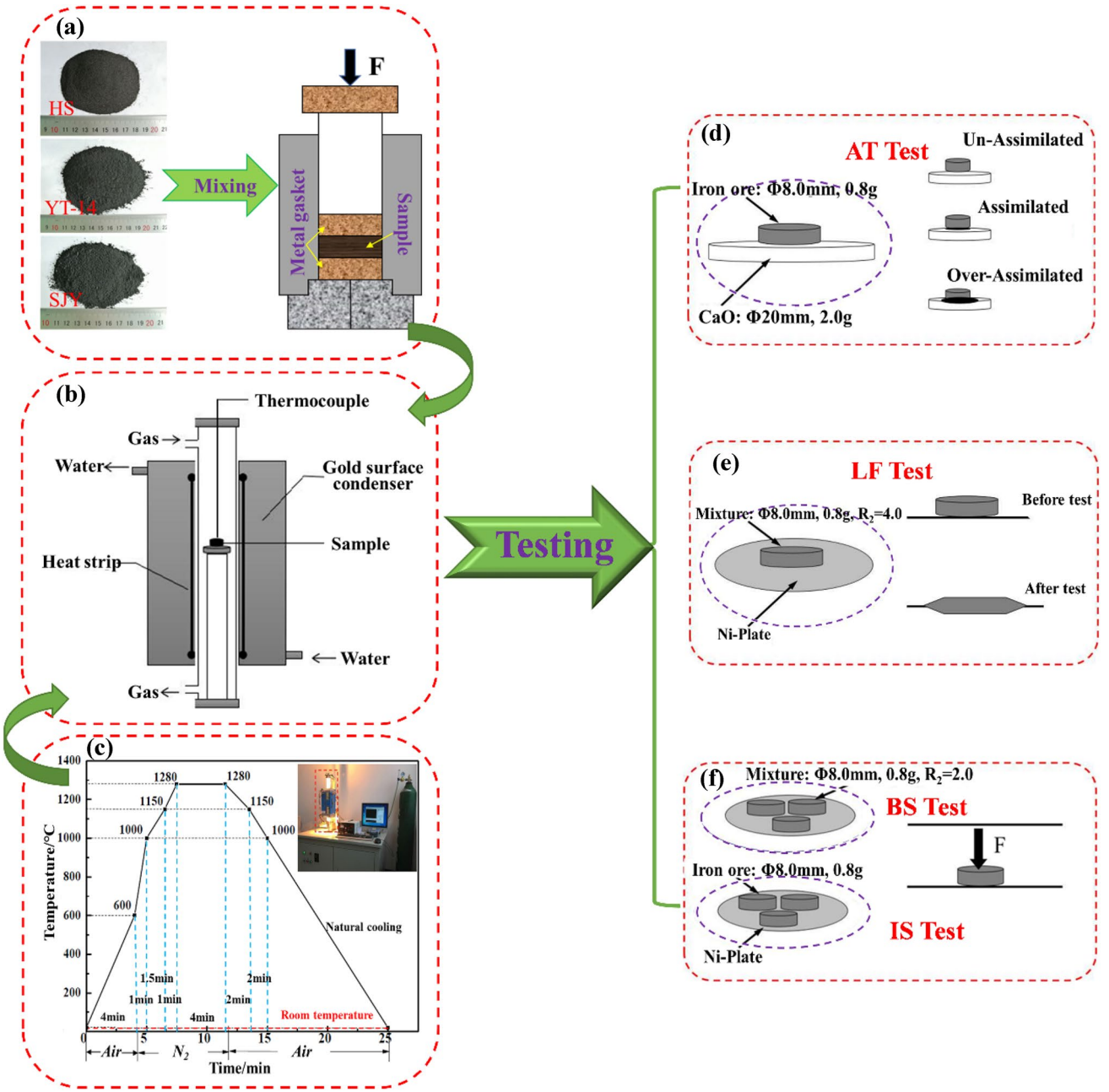

Fig. 2 Flowchart of high-temperature sintering experiment: **a** Sample preparation; **b** Experimental equipment; **c** Heating curve; **d** AT Test; **e** LF Test; **f** BS Test and IS Test

Different iron ore powders have different sintering behavior at high temperature. The determination of high-temperature sintering characteristics of iron ore powder is helpful to understand its physicochemical properties at high temperatures and the formation mechanism of the liquid phase. The assimilation temperature (AT) refers to the reaction ability of iron ore powder with CaO in the sintering process, which represents the difficulty of iron ore powder to form a liquid phase in the sintering process [14, 15]. Figure 2d shows the detection method of assimilation temperature. The liquid phase fluidity index (LF) refers to the fluidity of the liquid phase generated by the reaction between iron ore powder and CaO in the sintering process, which represents the effective bonding range of the binder phase [14, 15]. Figure 2e shows the detection method of the liquidity index, and the calculation formula of the fluidity index is shown in Eq. (1).

$$\text{Liquid phase fluidity index (LF)} = \frac{S_{\text{after}} - S_{\text{before}}}{S_{\text{before}}}, \quad (1)$$

where S_{before} is the vertical projection area of the adhering fines cylinder before the test (mm^2); S_{after} is the vertical projection area of the melt after the test (mm^2).

The binder phase strength (BS) represents the effective consolidation ability of the binder phase formed in the sintering process of iron ore powder to its surrounding iron ore particles. The intergranular consolidation strength (IS) represents the ability of minerals formed by intergranular consolidation under the high-temperature state of the sintering process. Figure 2f shows the detection method of binder phase strength and intergranular consolidation strength, whose indexes are expressed in the form of compressive strength of sintered block [14, 15].

In order to better study the high-temperature sintering characteristics and the formation mechanism of the liquid phase of sea sand vanadium titanomagnetite in the sintering process, the phase composition of high-temperature sintered blocks with sea sand ore was analyzed by XRD (X'Pert Pro; PANalytical, Almelo, the Netherlands), and the microstructure of high-temperature sintered blocks with sea sand ore was detected by SEM (Ultra Plus; Carl Zeiss GmbH, Jena, Germany) with a backscattering detector (BSE) and EDS.

Results and Discussion

High-Temperature Sintering Characteristics of Sea Sand Ore

Based on the particularity of chemical composition and particle morphology of sea sand vanadium titanomagnetite, and YT-14 and SJY ore used in the experiment, the high-temperature sintering characteristics of experimental materials, such as assimilation temperature (AT), liquid phase fluidity index (LF), binder phase strength (BS) and intergranular consolidation strength (IS), were studied by micro-sintering experiment. The experimental results are shown in Table 2.

It can be observed from the data in the table that the assimilation temperature of sea sand vanadium titanomagnetite was relatively high, which was 1290 ℃, which indicates that it is difficult to form a low-melting point liquid phase when the sea sand ore reacted with CaO in the sintering process. The assimilation temperature of SJY ore was the lowest (1230 ℃). The liquid phase fluidity index of sea sand ore and YT-14 was almost 0.00, which indicates that the fluidity of liquid phase formed by sea sand ore and YT-14 with CaO in the sintering process was poor, which was not conducive to improve the consolidation strength of sinter. The binder phase strength of sea sand ore was low, which was 145 N, which indicates that the liquid phase formed in the high-temperature sintering process of sea sand ore had a poor consolidation strength to surrounding particles. The intergranular consolidation strength of sea sand ore was also low, only 132 N, which indicates that the strength of sea sand ore particles obtained by crystal bond connection in the sintering process was poor. However, the intergranular consolidation strength of YT-14 and SJY were 6219 N and 3783 N, respectively.

Table 2 The high-temperature sintering characteristics of experimental materials

Materials	AT (℃)	LF	BS (N)	IS (N)
Sea sand ore	1290	0.00	145	132
YT-14	1280	0.00	3969	6219
SJY	1230	0.52	2178	3783

The high-temperature sintering characteristics of sea sand ore were studied by micro-sintering experiments. It can be found that the overall index was poor, and the quality of sinter prepared from sea sand ore was difficult to meet the requirements of blast furnace. Therefore, it was necessary to mix the iron ore powder with better high-temperature sintering characteristics with sea sand ore, to achieve the balance of advantages and disadvantages of high-temperature sintering characteristics and reach the standard of sinter.

Optimization of High-Temperature Sintering Characteristics by Adding Limestone

According to the high-temperature sintering characteristics of sea sand ore, its assimilation temperature was high and its liquid phase fluidity was poor. Therefore, limestone was added in the experiment to explore the reactivity between sea sand ore and CaO. The effect of limestone dosage on high-temperature sintering characteristics of sea sand ore is shown in Fig. 3.

The experimental results show that with the increase of limestone dosage, the assimilation temperature of sea sand ore was basically maintained at 1310 ℃, the liquid phase fluidity index increased gradually, the binder phase strength decreased gradually, and the intergranular consolidation strength increased first and then decreased. When the dosage of limestone was 4 wt%, the maximum intergranular consolidation strength was 10,155 N, the binder phase strength was still 3830 N, the assimilation temperature was 1310 ℃, and the liquid phase fluidity was 0.0934. Therefore, the appropriate dosage of limestone is 4 wt% in the sintering process of sea sand ore.

Optimization of High-Temperature Sintering Characteristics by Adding Ludwigite

According to the chemical composition of ludwigite in Table 1, its total iron content is 51.47 wt%, and it contains 6.34 wt% of low-melting compound B_2O_3, which can reduce

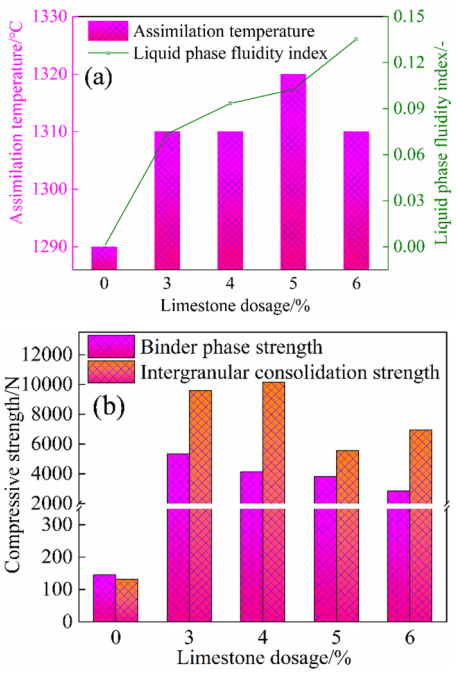

Fig. 3 Effect of limestone dosage on high-temperature sintering characteristics of sea sand ore: **a** AF and LF; **b** BS and IS

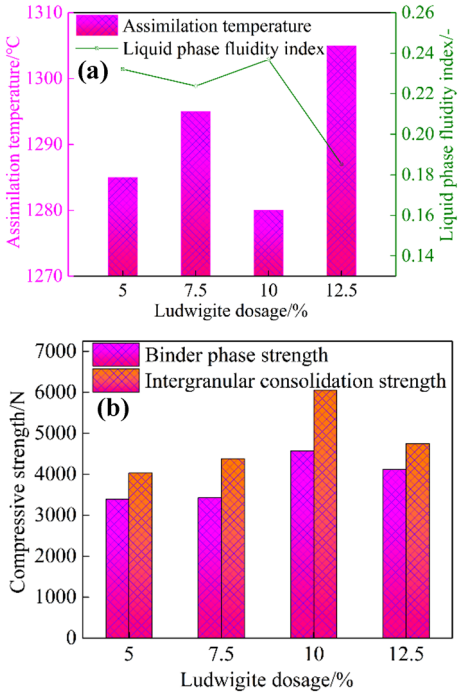

Fig. 4 Effect of ludwigite dosage on high-temperature sintering characteristics of sea sand ore: **a** AF and LF; **b** BS and IS

the assimilation temperature of sinter and improve the liquid phase consolidation ability. In addition, it also contains 12.65 wt% MgO, which belongs to polymetallic symbiotic iron ore. Therefore, a certain amount of ludwigite can be added to optimize the high-temperature sintering characteristics of sea sand ore. The effect of ludwigite dosage on high-temperature sintering characteristics of sea sand ore is shown in Fig. 4.

The experimental results show that with the addition of ludwigite from 5 to 12.5 wt%, the binder phase strength and intergranular consolidation strength of sinter increased gradually. When the dosage of ludwigite was 10 wt%, the assimilation temperature of sinter was lowest (1280 ℃), the liquid phase fluidity index attained a maximum of 0.2369, and the binder phase strength and intergranular consolidation strength were 4571 N and 6053 N, respectively. When the dosage of ludwigite continued to increase to 12.5 wt%, the overall index of high-temperature sintering characteristics of sinter became worse. Therefore, the high-temperature sintering characteristics of sea sand ore can be optimized to a certain extent by adding appropriate amount of ludwigite. According to the experimental results, the optimum dosage of ludwigite is 10 wt%.

Optimization of High-Temperature Sintering Characteristics by Adding Fine Powder

Based on the problem that sea sand ore particles are relatively coarse and ellipsoidal, which is not conducive to granulation, the SJY ore with fine particle size was selected as fine powder in the experiment. Based on optimizing the particle size of the mixed ore powder, the fine powder also improved the high-temperature sintering characteristics of the sinter. The effect of fine powder dosage on high-temperature sintering characteristics of sea sand ore is shown in Fig. 5.

The experimental results show that with the dosage of fine powder was gradually increased from 5 to 20 wt%, the liquid phase fluidity index of the sinter gradually increased, while the binder phase strength was maintained at 2200 N, and its intergranular consolidation strength was about 2800 N. When the dosage of fine powder was 20 wt%, the binder phase strength and the intergranular consolidation strength reached the maximum, which were 2345 N and 2907 N, respectively. At this time, the assimilation temperature was 1335 ℃, which was 10 ℃ higher than when the dosage of fine powder was 5 wt%, and the liquid phase fluidity index reached the maximum, which was 0.5904. Therefore, the optimal dosage of fine powder added in the sintering process is 20 wt%.

Effect of Sea Sand Dosage on High-Temperature Sintering Characteristics

The high-temperature sintering characteristics of sea sand ore were studied by micro-sintering experiments. To explore the optimal dosage of sea sand ore in the sintering process,

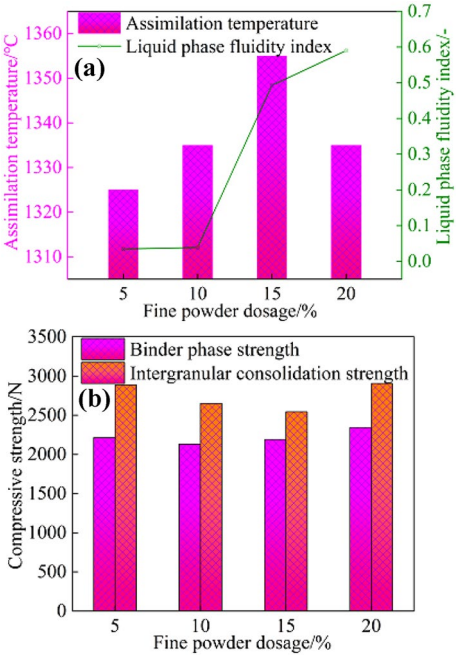

Fig. 5 Effect of fine powder dosage on high-temperature sintering characteristics of sea sand ore: **a** AF and LF; **b** BS and IS

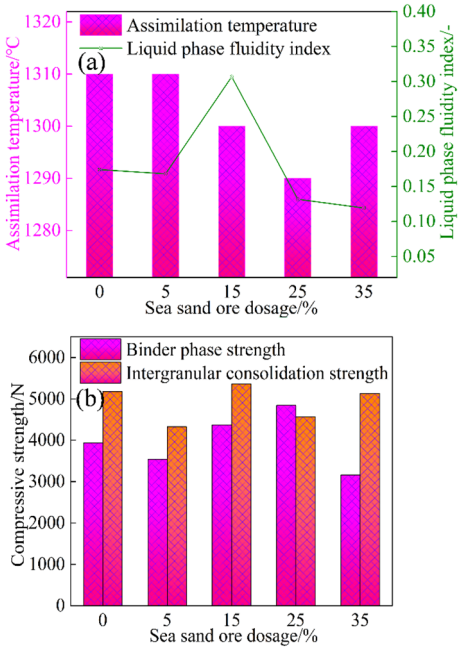

Fig. 6 Effect of sea sand ore dosage on high-temperature sintering characteristics: **a** AF and LF; **b** BS and IS

the ludwigite was fixed at 10 wt%, limestone at 4 wt%, PB powder at 51 wt%, and the amounts of sea sand ore and YT-14 ore were varied. The effect of sea sand ore dosage on high-temperature sintering characteristics is shown in Fig. 6.

The experimental results show that with the addition amount of sea sand ore gradually increased from 5 to 35 wt%, the assimilation temperature of the sinter was maintained at 1300 ℃, while the liquid phase fluidity index, binder phase strength, and intergranular consolidation strength all show a trend of first increasing and then decreasing. When the addition amount of sea sand ore was 15 wt%, the liquid phase fluidity index and the intergranular consolidation strength reached the maximum, which were 0.3067 and 5361 N, respectively. The maximum value of the binder phase strength was 4842 N, and the addition amount of sea sand ore was 25 wt%. When the added amount of sea sand ore was 35 wt%, the various indexes of high-temperature sintering characteristics showed a downward trend, but they were still in the appropriate range. Therefore, the appropriate dosage of sea sand ore in the sintering process should be 15–35 wt%, but subsequent sintering cup experiments should be carried out on this basis to further verify the appropriate dosage of sea sand ore.

Mechanism Analysis of High-Temperature Sintering

In order to study the sintering behavior and formation mechanism of the liquid phase at high temperature, the microstructure of sintered block, the intergranular consolidation strength, and the binder phase strength were studied with the help of SEM–EDS. The results are shown in Figs. 7 and 8. The chemical compositions of different sinters are shown in Tables S1–S4 of the electronic supplementary material.

According to Fig. 7a–c, the microstructure of the sintered block with sea sand ore in the intergranular consolidation strength test process shows that with the increase of the sea sand ore ratio, the number of pores in the sintered block showed a trend of slight increase, but the size of the pore gradually became smaller. The liquid phase area of the sintered block gradually decreased and showed a trend of dispersive distribution. According to the analysis of EDS (Fig. 7d), the liquid phase formed by the sintered block was mainly the gangue phase (P-a1, P-b1, P-c1,) containing Ca, Si, Al, and Mg showing a linear structure. The iron oxide phase mainly contained metal elements such as Fe, V, and Ti (P-a2, P-b2, P-c2,), showing an irregular block structure. This is mainly because the proportion of sea sand ore containing V_2O_5 and TiO_2 increased, the amount of liquid phase decreased, and the porosity increased. The brittle and hard perovskite may be generated in the sintering process, which was distributed between the liquid phase and iron oxide phase, thus weakening the bonding effect of the liquid phase and the intergranular consolidation effect of the iron oxide phase [29–31].

According to Fig. 8a–c, the microstructure of the sintered block with sea sand ore in the binder phase strength test process shows that when the basicity $R_2 = 2.0$, with the proportion of sea sand ore gradually increased, the number of pores

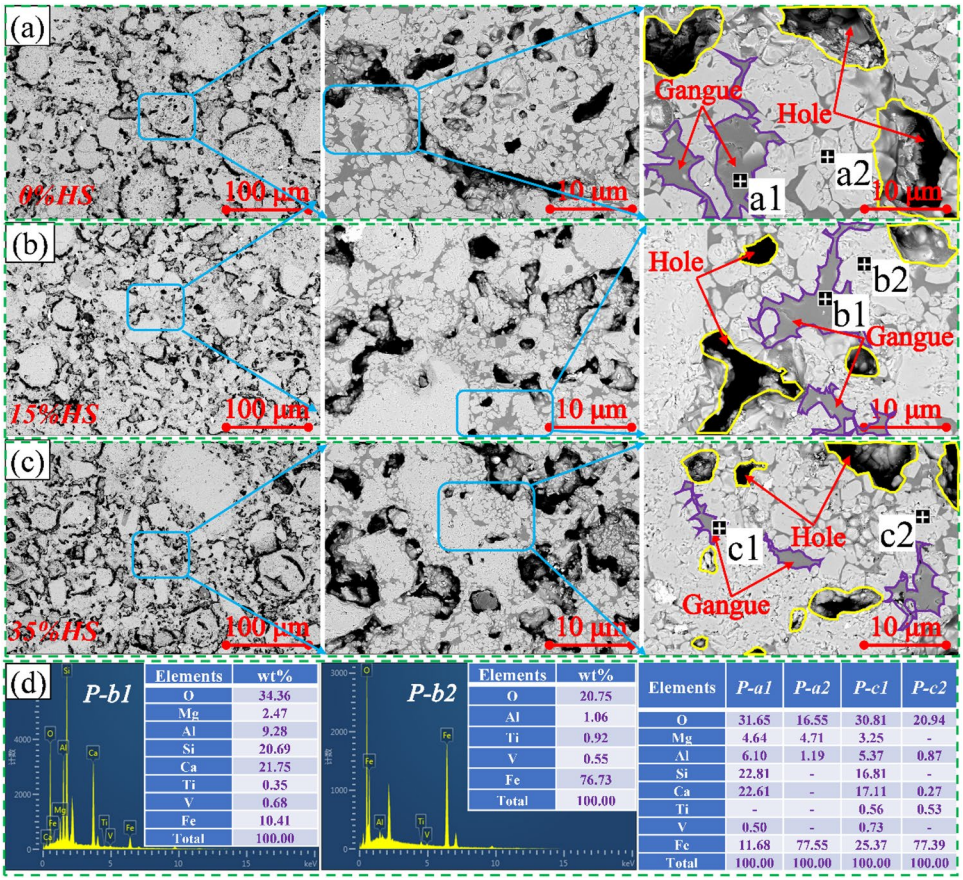

Fig. 7 SEM–EDS diagrams of sintered block with sea sand ore in the intergranular consolidation strength test process: **a** 0 wt% HS; **b** 15 wt% HS; **c** 35 wt% HS; **d** EDS analysis at the points 1 and 2 in a to c

in the sintered block showed a trend of slight decrease, but the size of the pores gradually increased, the distribution of liquid phase in the sintered block became more concentrated, and the complex calcium ferrite phase (SFCA) gradually appeared. This is mainly because, at basicity $R_2 = 2.0$, the effect of increased TiO_2 content on the sintered block was not as obvious as that of CaO. According to the analysis of EDS (Fig. 8d) and element distribution diagram (Fig. 8e), the main mineral components of the sintered block were gangue phase (containing a certain amount of Ca, Si, Al, Mg, P-a1, P-b1, P-c1), iron oxide phase (solid solution of a certain amount of V, Ti, P-a2, P-b2, P-c2), and SFCA phase (P-a3, P-b3, P-c3). According to the analysis of mineral microstructure, the gangue phase mainly showed a linear distribution, and the iron oxide phase showed an irregular block structure. When the proportion of sea sand ore was 35 wt%, the amount of gangue phase decreased, while the amount of SFCA phase increased rapidly, showing an irregular polygonal or columnar structure. The consolidation mode of the sintered block gradually transformed from the point-surface combination of the binder phase and iron oxide phase to the melt-interweaving consolidation of the SFCA and iron oxide phase.

XRD was used to analyze the phase of sintered block with sea sand ore in the binder phase strength test process, and the results are shown in Fig. 9. At basicity (R_2) of 2.0, the main phases were Fe_2O_3 (Maghemite, PDF # 01-089-0599), Fe_9TiO_{15} (Iron Titanium Oxide, PDF # 00-054-1267), Fe_3BO_6 (Iron Borate, PDF # 01-073-1385), Mg_2VO_4 (Magnesium Vanadium Oxide, PDF # 01–089-7411), $MgAl_{0.2}Fe_{1.8}O_4$ (Magnesium Aluminum Iron Oxide, PDF # 01–071-1233), SFCA (Calcium Iron Oxide, PDF # 01–089-8664), and silicate phase. Since the contents of SiO_2 and Al_2O_3 in sea sand ore are 3.27 wt% and 3.33 wt%, respectively, while the contents of SiO_2 and Al_2O_3 in YT-14 are 1.83 wt% and 1.41 wt%, respectively, the contents of SiO_2 and Al_2O_3 in sintered block increased with the increase of sea sand ore ratio. Therefore, with the increase in sea sand ore dosage, the silicate phase was transformed from $CaAl_4Fe_8O_{19}$ (Calcium Aluminum Iron Oxide, PDF # 00-049-1586) with $2\theta = 24.184°$ to $CaFe(Si_2O_6)$ with $2\theta = 30.167°$ (Calcium Iron Silicate, PDF # 01-087-1700), and the $MgAl_{0.2}Fe_{1.8}O_4$ (Magnesium Aluminum Iron Oxide, PDF # 01-071-1233) phase containing Al appeared at $2\theta = 43.151°$. According to the above XRD diagram analysis, the reactions that may occur in the sintering process are shown in Eq. (2)–(8).

$$Fe_3O_4 + 1/4O_2 = 3/2Fe_2O_3 \quad (2)$$

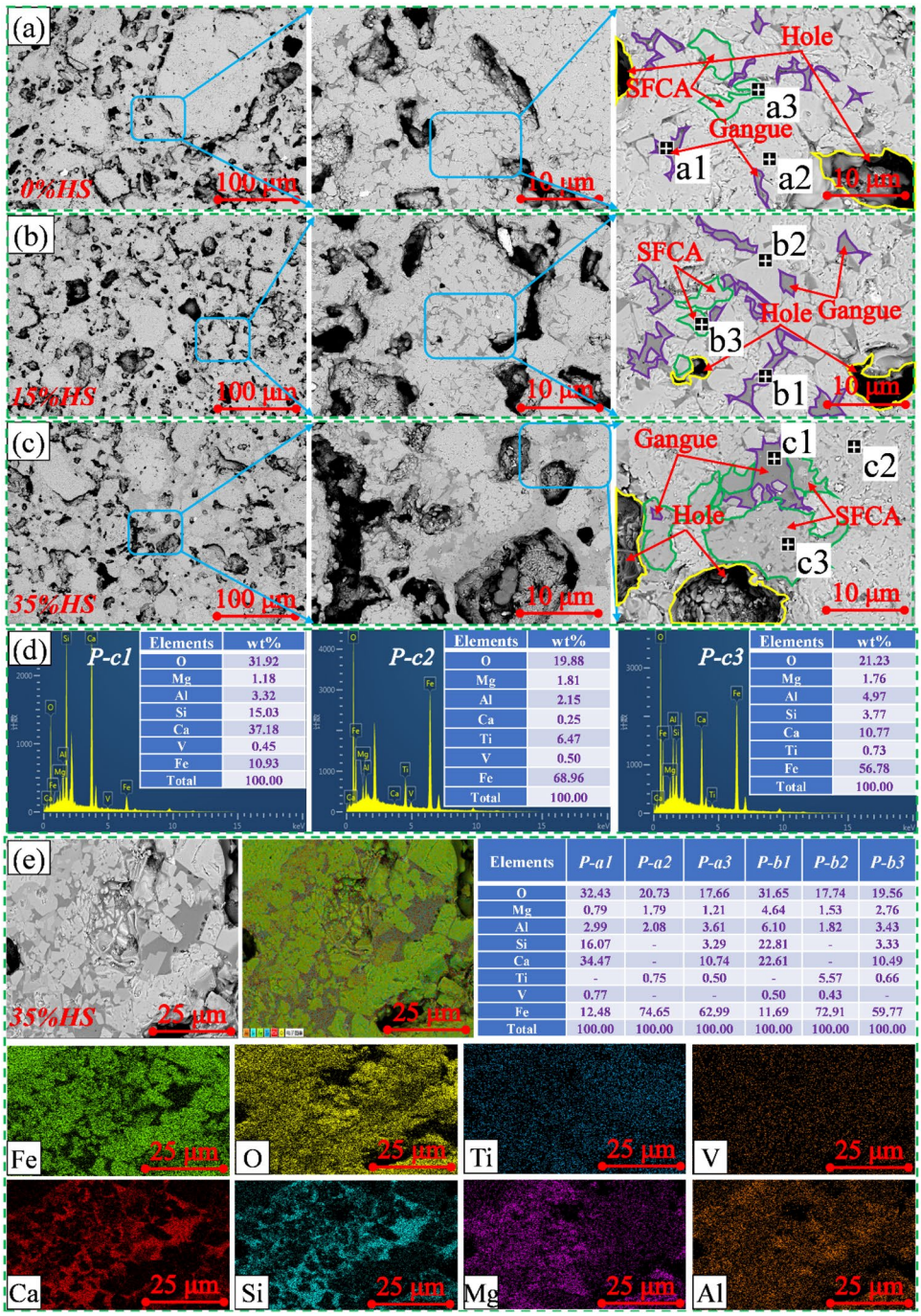

Fig. 8 SEM–EDS diagrams of sintered block with sea sand ore in the binder phase strength test process: **a** 0 wt% HS; **b** 15 wt% HS; **c** 35 wt% HS; **d** EDS analysis at the point 1, 2, and 3 in a to c; **e** element distributions of sintered blocks with 35 wt% sea sand ore

$$Fe_2TiO_4 + 7/3Fe_3O_4 + 5/6O_2 = Fe_9TiO_{15} \quad (3)$$

$$Fe_2O_3 + 1/3B_2O_3 = 2/3Fe_3BO_6 \quad (4)$$

$$MgO + 1/8V_2O_3 + 1/8V_2O_5 = 1/2Mg_2VO_4 \quad (5)$$

$$CaO + FeO + 2SiO_2 = CaFe(Si_2O_6) \quad (6)$$

$$MgO + 1/10Al_2O_3 + 9/10Fe_2O_3 = MgAl_{0.2}Fe_{1.8}O_4 \quad (7)$$

$$CaO + 2Al_2O_3 + 4Fe_2O_3 = CaAl_4Fe_8O_{19} \quad (8)$$

Based on the analysis of the above results, a schematic diagram for the high-temperature sintering mechanism of sintered block with sea sand ore in different proportions can be obtained as shown in Fig. 10. It can be observed from

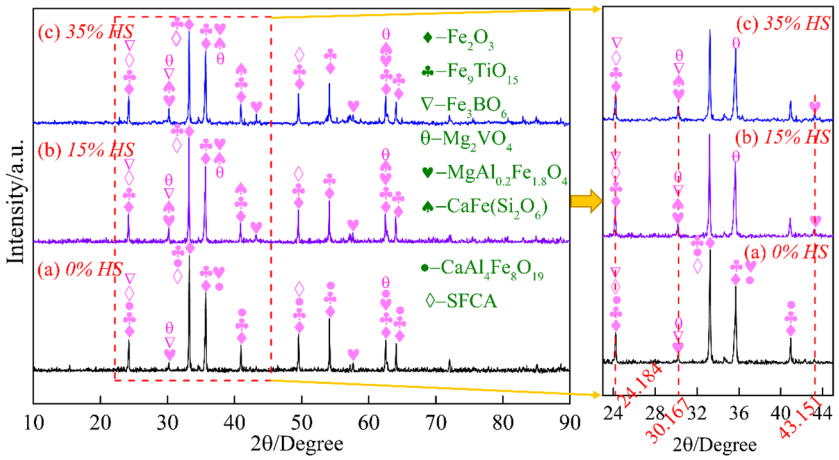

Fig. 9 XRD diagram of sintered block with sea sand ore in the binder phase strength test process

Fig. 10a that in the intergranular consolidation strength test process of sintered block with sea sand ore, the intergranular consolidation method of the sintered block was mainly the point-surface combination of the binder phase and iron oxide phase. With the proportion of sea sand ore increased from 0 to 35 wt%, the content of TiO_2 in sintered block increased, the amount of sintering liquid phase decreased, and the distribution was more dispersed, the size of the pores decreased gradually, but the porosity increased, which weakened the bonding effect of liquid phase and the intergranular consolidation effect of iron oxide phase. It can be observed from Fig. 10b that the effect of CaO on the microstructure of the sintered block with sea sand ore was more obvious in the binder phase strength test process of sintered block with the basicity $R_2 = 2.0$. When the proportion of sea sand ore was increased from 0 to 35 wt%, the amount of sintering liquid phase decreased, but it was more concentrated. The size of the pores gradually increased, and the amount of SFCA phase rapidly increased. The consolidation mode of the sintered block gradually transformed from the point-surface combination of the binder phase and iron oxide phase to the melt-interweaving consolidation of the SFCA and iron oxide phase.

Conclusions

In view of sea sand vanadium titanomagnetite has the problem of poor sintering performance, the high-temperature sintering characteristics of sea sand ore, Yuantong-14 (YT-14) and Sijiaying (SJY) were studied by micro-sintering experiment in this paper. The high-temperature sintering characteristics of sea sand vanadium titanomagnetite were optimized by different methods in order to improve the utilization rate of sea sand ore. Based on this research, the following conclusions are drawn:

(1) The high-temperature sintering characteristics of sea sand ore were the worst, and the high-temperature sintering characteristics of sea sand ore can be optimized to a certain extent by adding 4 wt% limestone, 10 wt% ludwigite, and 20 wt% fine powder (SJY).

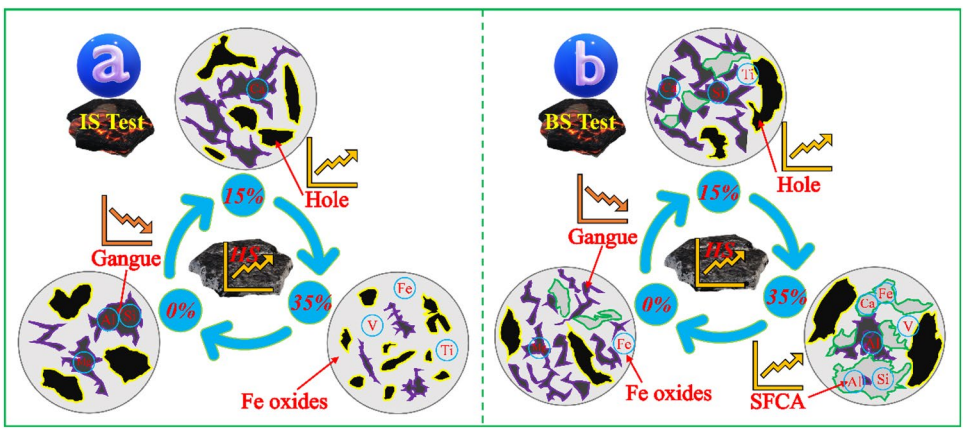

Fig. 10 Schematic diagram for the high-temperature sintering mechanism of sintered blocks with sea sand ore in different proportions: **a** IS test; **b** BS test

(2) At the dosing rates of 4 wt% limestone, 10 wt% ludwigite, and 51 wt% PB powder, and changing the dosage of sea sand ore and YT-14 ore, the high-temperature sintering performance of sinter with 15–35 wt% sea sand ore was still in the appropriate range.

(3) According to the analysis of mineral phase composition and microstructure of sintered block with sea sand ore, with the proportion of sea sand ore increased from 0 to 35 wt%, the consolidation mode of the sintered block gradually transformed from the point-surface combination of the binder phase and iron oxide phase to the melt-interweaving consolidation of the SFCA and iron oxide phase.

(4) This study provides theoretical guidance and reference methods for the preparation of the sinter from sea sand. According to the experimental results, the utilization rate of sea sand ore can be increased to 35 wt%. However, in view of the poor pelletizing and sintering performance of sinter with sea sand ore, the follow-up work should focus on the research on the metallurgical properties of sea sand sinter in the blast furnace smelting process.

Supplementary Information The online version contains supplementary material available at https://doi.org/10.1007/s40831-022-00570-4.

Acknowledgements The authors are especially thankful to the National Natural Science Foundation of China (Grant Nos. 51674084, 21908020, and U1908226) and Fundamental Research Funds for the Central Universities (Grant No. N182503035).

Declarations

Conflict of interest The authors declare that they have no conflict of interest.

References

1. Lu YN, Wu SL, Zhou H, Ma LM, Liu ZJ, Wang Y (2021) Effect of Ti–V Magnetite concentrate pellet on the strength of green pellets and the quality of sinter by composite agglomeration process (CAP). ISIJ Int 61(8):2211–2219. https://doi.org/10.2355/isijinternational.ISIJINT-2021-005
2. Du HG (1996) Principle of smelting vanadium-titanium magnetite in the blast furnace, 1st edn. Science Press, Beijing, China, p 1
3. Cheng GJ, Xue XX, Jiang T, Duan PN (2016) Effect of TiO_2 on the crushing strength and smelting mechanism of high-chromium vanadium-titanium magnetite pellets. Metall Mater Trans B 47(3):1713–1726. https://doi.org/10.1007/s11663-016-0628-7
4. Cheng GJ, Xing ZX, Yang H, Xue XX (2021) Effects of high proportion unground sea sand ore on the preparation process and reduction performance of oxidized pellets. Minerals 11(1):87–103. https://doi.org/10.3390/min11010087
5. Wright JB (1967) Heating experiments on New Zealand ironsands and the presence of pseudobrookite. N Z J Geol Geophys 10(3):659–665. https://doi.org/10.1080/00288306.1967.10431084
6. Xing ZX, Cheng GJ, Gao ZX, Yang H, Xue XX (2020) Optimization of experimental conditions on preparation of oxidized pellets with New Zealand Sea sand ore. Metall Res Technol 117:411–421. https://doi.org/10.1051/metal/2020043
7. Xing ZX, Cheng GJ, Yang H, Xue XX (2019) Experimental research on preparation of oxidized pellets with high proportion sea sand mine. In: The 12th CSM steel congress, Beijing, vol 10, pp 122–125. https://doi.org/10.26914/c.cnkihy.2019.058725.
8. Wang Z, Pinson D, Chew S, Rogers H, Monaghan BJ, Pownceby MI (2016) Behavior of New Zealand irons and during iron ore sintering. Metall Mater Trans B 47:330–343. https://doi.org/10.1007/s11663-015-0519-3
9. Xing ZX, Cheng GJ, Gao ZX, Yang H, Xue XX (2021) Effect of incremental utilization of unground sea sand ore on the consolidation and reduction behavior of Vanadia-Titania magnetite pellets. Metals 11(2):269–286. https://doi.org/10.3390/met11020269
10. Podder A (2021) Study of humidity on moisture transfer characteristics in iron ore sintering. Trans Indian Inst Met 74(6):1479–1487. https://doi.org/10.1007/s12666-021-02244-3
11. Park E, Ostrovski O (2004) Effects of preoxidation of Titaniaferrous ore on the ore structure and reduction behavior. ISIJ Int 44:74–81. https://doi.org/10.2355/isijinternational.44.74
12. Longbottom RJ, Monaghan BJ, Mathieson JG (2013) development of a bonding phase within titanomagnetite-coal compacts. ISIJ Int 53:1152–1160. https://doi.org/10.2355/isijinternational.53.1152
13. Geng C, Sun TC, Ma YW, Xu CY, Yang HF (2017) Effects of embedding direct reduction followed by magnetic separation on recovering titanium and iron of beach titanomagnetite concentrate. J Iron Steel Res Int 24:156–164. https://doi.org/10.1016/S1006-706X(17)30022-5
14. Wu SL, Dai YM, Dauter O, Pei YD, Xu J, Han HL (2010) Optimization of ore blending during sintering based on complementation of high temperature properties. J Univ Sci Technol Beijing 32(6):719–724. https://doi.org/10.13374/j.issn1001-053x.2010.06.006
15. Wu SL, Liu Y, Du JX, Mi K, Lin H (2002) New concept of iron ores sintering basic characteristics. J Univ Sci Technol Beijing 24(3):254–257. https://doi.org/10.13374/j.issn1001-053x.2002.03.048
16. Zhou H, Wang JK, Ma PN, Meng HX, Cheng FZ, Luo JW (2021) Influence of quick lime on pore characteristics of high-temperature zone in iron ore sinter based on XCT technology. J Mater Res Technol 15:4475–4486. https://doi.org/10.1016/j.jmrt.2021.10.061
17. Zhou M, Zhou H (2020) Experimental investigation and numerical modeling of strength properties of iron ore sinter based on pilot-scale pot tests and X-ray computed tomography. J Mater Res Technol 9:13106–13117. https://doi.org/10.1016/j.jmrt.2020.09.054
18. Xue YX, Pan J, Zhu DQ, Guo ZQ, Yang CC, Lu LM (2020) Improving high-alumina iron ores processing via the investigation of the influence of alumina concentration and type on high-temperature characteristics. Minerals 10(9):802–828. https://doi.org/10.3390/min10090802
19. Wu SL, Zhang GL (2015) Liquid absorbability of iron ores and large limonite particle divided adding technology in the sintering process. Steel Res Int 86(9):1014–1021. https://doi.org/10.1002/srin.201400300
20. Wu SL, Su B, Qi YH, Kou MY, Li Y, Zhang WL (2017) Melt absorbability of iron ore nuclei and its influence on suitable liquid content of sintered body. Metall Mater Trans B 48(5):2469–2480. https://doi.org/10.1007/s11663-017-1059-9

21. Zhai XB, Wu SL, Zhou H, Su LX, Ma XD (2020) Flow and penetration behaviours of liquid phase on iron ore substrate and their effects on bonding strength of sinter. Ironmak Steelmak 47(4):405–416. https://doi.org/10.1080/03019233.2018.1537223
22. Liu DH, Liu H, Zhang JL, Liu ZJ, Xue X, Wang GW (2017) Basic characteristics of Australian iron ore concentrate and its effects on sinter properties during the high-limonite sintering process. Int J Miner Metall Mater 24(9):991–998. https://doi.org/10.1007/s12613-017-1487-1
23. Liu DH, Li JH, Peng Y, Zhang JL, Wang GW, Xue X (2019) Comprehensive evaluation of sintering basic characteristics of iron ore based on grey relational analysis. J Iron Steel Res Int 26:691–696. https://doi.org/10.1007/s42243-019-00259-1
24. Liu DH, Zhang JL, Liu ZJ, Wang YZ, Xue X, Yan J (2016) Effects of iron sand ratios on the basic characteristics of vanadium titanium mixed ores. JOM 68(9):2418–2424. https://doi.org/10.1007/s11837-016-1989-8
25. Zhang A, Monaghan BJ, Longbottom RJ, Nusheh M, Bumby CW (2020) Reduction kinetics of oxidized New Zealand ironsand pellets in H_2 at temperatures up to 1443 K. Metall Mater Trans B 51:492–504. https://doi.org/10.1007/s11663-020-01790-3
26. Sun HY, Wang JS, Han YH, She XF, Xue QG (2013) Reduction mechanism of titanomagnetite concentrate by hydrogen. Int J Miner Process 125(10):122–128. https://doi.org/10.1016/j.minpro.2013.08.006
27. Longbottom RJ, Ingham B, Reid MH, Studer AJ, Bumby CW, Monaghan BJ (2019) In situ neutron diffraction study of the reduction of New Zealand ironsands in dilute hydrogen mixtures. Miner Process Ext Metall 128(3):183–192. https://doi.org/10.1080/03719553.2017.1412877
28. Prabowo SW, Longbottom RJ, Monaghan BJ, Puerto D, Ryan MJ, Bumby CW (2021) Phase transformations during fluidized bed reduction of New Zealand titanomagnetite ironsand in hydrogen gas. Powder Technol. https://doi.org/10.1016/j.powtec.2021.117032
29. Tang WD, Yang ST, Cheng GJ, Gao ZX, Yang H, Xue XX (2018) Effect of TiO_2 on the sintering behavior of chromium-bearing vanadium-titanium magnetite. Minerals 8(7):263–277. https://doi.org/10.3390/min8070263
30. Bristow NJ, Loo CE (1992) Sintering properties of iron ore mixes containing titanium. ISIJ Int 32(7):819–828. https://doi.org/10.2355/isijinternational.32.819
31. Chiwandika EK, Jung SM (2020) Effects of ilmenite ore on phase development of hematite ore sinter. Metall Mater Trans B 51:1469–1484. https://doi.org/10.1007/s11663-020-01856-2

Authors and Affiliations

Zhenxing Xing[1,2] · Jie Ma[1,2] · Gongjin Cheng[1,2] · He Yang[1,2] · Xiangxin Xue[1,2,3,4]

✉ Xiangxin Xue
xuexx@mail.neu.edu.cn

[1] School of Metallurgy, Northeastern University, Shenyang 110819, People's Republic of China

[2] Liaoning Key Laboratory of Recycling Science for Metallurgical Resources, Shenyang 110819, People's Republic of China

[3] Northeastern University Innovation Research Institute of Vanadium and Titanium Resource Industry Technology, Shenyang 110819, People's Republic of China

[4] Innovation Research Institute of Comprehensive Utilization Technology for Vanadium-Titanium Magnetite Resources in Liaoxi District, Chaoyang 122000, People's Republic of China